Journal of Power Sources 212 (2012) 47–56

Contents lists available at SciVerse ScienceDirect

Journal of Power Sources

journal homepage: www.elsevier.com/locate/jpowsour

Tungsten carbide-based anodes for solid oxide fuel cells: Preparation, performance and challenges

Alireza Torabi*, Thomas H. Etsell

Department of Chemical & Materials Engineering, University of Alberta, Edmonton, Alberta T6G 2G6, Canada

ARTICLE INFO

Article history:
Received 25 January 2012
Received in revised form
30 March 2012
Accepted 31 March 2012
Available online 13 April 2012

Keywords:
Solid oxide fuel cells
Tungsten carbide anode
Methane fuel
Carbon formation
Infiltration

ABSTRACT

New materials based on WC-YSZ composites were investigated as potential anodes for direct methane-fueled solid oxide fuel cells (SOFCs). Two different carbide-based composites were developed in this study: a conventional WC-YSZ (50:50 vol.%) composite and an infiltrated WC-YSZ composite (20 vol.% WC infiltrated into a porous YSZ support). It was shown that a conventional WC-YSZ composite cannot be used as an alternative anode because of catastrophic changes in anode microstructure due to the carbide phase decomposition. The infiltrated WC-YSZ, however, performed rather stably with no catastrophic degradation at 800–900 °C under mixed hydrogen–methane and methane fuels. Furthermore, while WC-based anodes were resistance to carbon formation under methane, the fuel was poorly activated and the performance was quite low. The carbide-based electrodes were then modified by incorporation of 5 wt% CeO_2 and 1 wt% Ru. Not only did the addition of ceria–Ru electrocatalysts dramatically enhance the fuel cell performance, it also greatly improved the stability of the polarized cell. Both calculations and experiments showed that kinetic factors play the major role in stability of the carbide phase. It is proposed here that the carbide-infiltrated YSZ support can reasonably be considered as a foundation for future studies to develop promising alternative anodes.

1. Introduction

Ni-YSZ composites have been the dominant anodes of choice for solid oxide fuel cell applications for more than four decades [1–3]. This is mostly because of unrivaled attributes of such anodes including excellent catalytic activity toward hydrogen fuel, high electronic and sufficient ionic conductivity, and reasonable stability under SOFC operating conditions [3–5]. In addition, low cost, relative ease of fabrication and adequate mechanical strength are other practical contributing features of these cermets which make them even more attractive.

On the other hand, there are several limitations in regard to Ni-YSZ anode materials [6]. Incompatibility with hydrocarbon fuels is one of the most significant drawbacks of conventional Ni-YSZ anodes [7]. Nickel is an excellent catalyst for pyrolysis of hydrocarbon fuels [8]. As a result of such reaction, carbon is deposited on the Ni surface, dissolves into the Ni bulk and finally precipitates from it as fibers. Although several attempts have been made to improve the compatibility of the Ni-YSZ cermets and hydrocarbon fuels [9], the intrinsic instability of these anodes and disastrous consequences of the formation of carbon filaments limit the practicality of those attempts [7]. Other significant disadvantages of Ni-YSZ anodes includes high sensitivity to fuel impurities such as H_2S, CH_3SH, COS, NH_3 and Cl_2 [10], microstructural change due to Ni phase coarsening [11] and poor resistance against redox cycling [12].

Development of alternative anode materials is thus a practical approach to directly utilize hydrocarbon fuels. The alternatives include a variety of ceramic-metal composites and oxide ceramics [1,4–7]. Copper-based cermets have been extensively investigated as a potential candidate for direct hydrocarbon utilization [7,13]. The major advantage of Cu over Ni is that it does not promote the formation of carbon fibers. Kim et al. [14] showed that Cu–CeO_2-YSZ stably performed in a wide variety of hydrocarbons. While copper mainly contributes to electronic conductivity, the major role of ceria is to catalyze the oxidation of hydrocarbon fuel [13]. Although they are compatible with hydrocarbons, there are several drawbacks concerning Cu-based anodes [15]. First, the catalytic activity of copper toward hydrocarbon fuels is rather poor. Therefore, incorporation of active electrocatalysts into the copper-based electrodes is unavoidable. Second, because Cu has a relatively low melting point (1085 °C), long-term stability of these anodes at higher operating temperatures is a serious concern. Third, the

* Corresponding author. Tel.: +1 780 7070631; fax: +1 780 492 2881.
E-mail addresses: atorabit@gmail.com, torabite@ualberta.ca (A. Torabi).

0378-7753/$ – see front matter © 2012 Elsevier B.V. All rights reserved.
doi:10.1016/j.jpowsour.2012.03.102

conventional fabrication technique involving NiO which is used for Ni-based anodes cannot be used with Cu-based electrodes because of the low melting temperatures of copper oxides. Finally, these cermets are not compatible with precious metal catalysts such as Pd and Ru due to the formation of catalytically inactive alloys.

Other substitutes for the Ni-YSZ electrode are those based on oxide ceramics including fluorite- and perovskite-based structures [16,17]. Decent compatibility with oxide electrolytes, higher microstructural stability and resistance to redox cycling are the major benefits of this group of alternative anodes. On the other hand, the electronic conductivity of these oxides is several orders of magnitude lower than that of Ni-YSZ composite anodes. For the sake of comparison, the electronic conductivity of Ni-YSZ composite (50:50 vol.%), gadolinium doped ceria and yttrium doped strontium titanate are in the range of >1000, 0.1–1, and 1–100 S cm^{-1}, respectively, at 800 °C under reducing conditions [16–18]. Furthermore, although carbon formation and poisoning by fuel impurities are generally less problematic with oxides, the catalytic activity of the majority of oxide anodes toward alternative fuels is relatively low [7,17].

Ever since Levy and Boudart [19] reported the resemblance between Pt and tungsten carbide in surface catalysis, the catalytic characteristics of Groups IV–VI carbides have been the subject of numerous studies [20]. These investigations have shown that the catalytic characteristics of these carbides are comparable with those of Pt-group precious metals [20], especially in reactions which deal with the transformation of C–H bonds of hydrocarbons. In particular, carbides of molybdenum and tungsten have been extensively investigated as electrocatalysts for low temperature fuel cells including proton exchange membrane (PEM) and direct methanol (DM) fuel cells [21–23]. These carbide ceramics, however, have not been studied to any great extent as potential anode materials for SOFC applications.

To the best of our knowledge, the first attempt to study a tungsten carbide-based anode for SOFCs was made by Naoumidis et al. [24] in 1996. They reported that a WC-YSZ composite anode could potentially show a better performance than a Pt anode under 90% CO–10% CO_2 as the fuel. While they expressed concerns about the stability of the carbide phase, they proposed that WC is thermodynamically stable at $CH_4/H_2O > 0.2$ and concluded that with such anodes, a reasonable yield of oxidation products can be obtained. Ten years later, stability of a variety of metal carbides was investigated to develop sulphur tolerant materials for SOFCs anodes [25]. It was shown that except for the carbides of Mo and W, other metal carbides cannot be used as alternative materials for SOFC anodes, solely because the corresponding oxides are much more stable under typical SOFC anode atmospheres.

Recently, we performed extensive symmetrical cell studies to investigate the electrochemical behavior of tungsten carbide-based materials for SOFC anodes [26]. The compelling attributes of WC which motivated us included catalytic resemblance between the carbide and precious metals, very high electronic conductivity (same order of magnitude as metals) and very high melting point (2870 °C) which guarantees the microstructural stability during cell operation. Our preliminary results revealed that the ohmic polarization of WC-YSZ composite is comparable to that of Ni-YSZ cermets. The non-ohmic polarization, however, is relatively large and the incorporation of active electrocatalysts is unavoidable, particularly under methane fuel. We showed that addition of 10 wt % ceria and 3 wt% ruthenium into the WC-YSZ electrode remarkably improves the electrochemical performance.

In this study, we report the performance of solid oxide fuel cells based on WC-YSZ composite anodes under mixed hydrogen–methane and methane fuels. First, the preparation of a conventional WC-YSZ and a WC-infiltrated YSZ porous support is explained in detail. Then the cell performance of these conventional and infiltrated cells is compared and the effect of ceria and Ru addition into the carbide-based electrode is described. Lastly, the implications of these results and the challenges of WC-based anodes are discussed.

2. Experimental procedure

2.1. Cell fabrication

YSZ discs (FuelCellMaterials, Lewis Center, OH, diameter: 25 mm, average thickness: 0.3 mm) were used as the electrolyte as well as the mechanical support. Two different carbide-based anodes were studied in this work: conventional WC-YSZ composite- and infiltrated WC-YSZ-based materials. To prepare the former, tungsten carbide (WC) was obtained from Inframat Advanced Materials, Manchester, CT (nanocrystalline tungsten carbide powder, 99.95%, particle size: 200 nm, crystal size: 40–70 nm) and yttria-stabilized zirconia (YSZ) was supplied by FuelCellMaterials, Lewis Center, OH (yttria-stabilized zirconia 8 mol %, fine grade (YSZ8-U1), particle size: 300–500 nm). 7.26 g of the carbide and 2.74 g of the oxide (equal volume percentage of WC and YSZ) were put into a 50 mL polypropylene jar. 10 g of zirconia balls (Tosoh YTZ grinding media, 3 mm) and 10 mL of ethanol were added and they were mixed for an hour at 500 rpm using the planetary ball mill. Once the mixture was dried, 10 g of the laboratory-made ink was added to 10 g of the composite powder and they were well mixed in a mortar and pestle for 30 min. WC-YSZ anodes (diameter: 10 mm, average thickness: 25 μm) were then screen printed onto the YSZ discs. The coated discs were dried at 150 °C for 15 min and sintered at 1300 °C for 3 h under 1000 ppm CO_2, balance CO.

In this study, for the infiltrated composite anodes and for the cathodes, a thin porous YSZ scaffold is used as a support. Calcined-milled YSZ (CYSZ) powder was used as the starting material to make the porous support. To prepare the CYSZ powder, as-received YSZ (Tosoh TZ-8Y, Grove City, OH) was heat treated at 1500 °C for 3 h. 50 g of CYSZ, 300 g of zirconia balls (Tosoh YTZ grinding media, 5 mm) and 50 mL of distilled water were mixed in a 250 mL polypropylene jar and the mixture ball milled for 72 h at 80 rpm. The suspension was then dried at 120 °C for 24 h and the dried agglomerates were manually ground in an alumina mortar and pestle for half an hour. To prepare CYSZ paste, 10 g of CYSZ powder, 0.5 g (20 vol.%) of polymethyl methacrylate ((PMMA), Microbeads®, Spheromers CA 6, Norway) as a pore former, 10 g of zirconia balls (Tosoh YTZ grinding media, 3 mm) and 10 mL of ethanol were added into a 50 mL polypropylene jar and they were mixed for an hour at 500 rpm using a planetary ball mill (Retsch, PM 100). After drying the mixture, a laboratory-made ink (α-terpineol + 5 wt% ethylcellulose) was added (10 g powder + 10 g ink) and they were well mixed in the mortar and pestle for 30 min. YSZ coatings (diameter: 10 mm, average thickness: 25 μm) were then screen printed onto YSZ discs and sintered at 1300 °C for 3 h.

To prepare the WC-infiltrated porous YSZ electrodes, ammonium metatungstate (AMT) was used (Inframat Advanced Materials, Manchester, CT) as the starting precursor. 1 g of distilled water was added to 3 g of the precursor in a 10 mL glass container. Using a regular laboratory ultrasonic cleaner for 10 min, AMT was completely dissolved in the water to leave a clear solution. 0.15 g of Triton (X-45, Union Carbide Chemicals and Plastics Co. Inc., Danbury, CT) was then mixed into the solution to play a role as a surfactant. The solution was heated up to 100 °C in an oil bath and this hot solution was infiltrated into the preheated (150 °C) porous YSZ electrode coatings. The impregnated discs were then heat treated at 350 °C for 15 min. This procedure was repeated (twice on

average) until 20 vol.% WC was embedded into the YSZ network. To synthesize the carbide phase, the infiltrated discs were heated to 600 °C in air. Ar was then introduced to flush out the air and lastly an 80% H_2–20% CH_4 atmosphere was introduced. The final heat treatment condition was 880 °C for 12 h. A heat treated coating was examined by X-ray diffraction (XRD, Rigaku Ultima IV) which confirmed the presence of a nano-sized WC phase along with YSZ.

To investigate the effect of other active electrocatalysts on the electrochemical performance of WC-YSZ cells, they were infiltrated with ceria and/or Ru. A 0.25 M solution of cerium ammonium nitrate (Alfa Aesar) in ethanol was prepared as a precursor for ceria. The WC-YSZ support was infiltrated with the ceria solution using a micro-syringe and subsequently dried at 150 °C for 15 min followed by a heat treatment at 350 °C for another 15 min. The infiltration-heat treatment cycle was repeated 10 times to obtain 5 wt% ceria. Similarly, a 0.1 M solution of $RuCl_3 \cdot xH_2O$ ($x \leq 1$) (Sigma–Aldrich) in ethanol was prepared. The support was then impregnated by this solution using a micro-syringe and dried at 150 °C for 15 min. The impregnation was repeated five times and the final Ru gain was about 1 wt%.

Since the focus of this work is on the anode, Pt was initially picked as the cathode of choice. Platinum paste was obtained from Heraeus Materials Technology LLC, West Conshohocken, PA (OS2, CL11-5349). The cathode performance was, however, poor. Thus, $La_{0.8}Sr_{0.2}MnO_3$ (LSM), as a well studied cathode material, was chosen to be infiltrated into the porous YSZ structure on the cathode side. $Mn(NO_3)_2 \cdot xH_2O$, $La(NO_3)_3 \cdot 6H_2O$, and $Sr(NO_3)_2$ from Alfa Aesar were used as the starting precursors to prepare a solution based on Pechini's method [27]. The molar ratio of metal cations, complexing agent (citric acid) and ethylene glycol in the solution was 1:4:4. A small amount of the solution was dried and then heated to 700 °C in air. The synthesized powder was examined by XRD which confirmed the presence of LSM as the only phase. The thin porous support was repeatedly impregnated by incipient wetness (10 times, on average) until 20 vol.% LSM was embedded into the YSZ network with the LSM phase to be formed in-situ.

2.2. Cell test

A laboratory-made gold paste was used as a current collector (atomized gold powder, Technic Inc., Cranston, Rhode Island) on both cathode and anode sides. The anode side of the cell was sealed onto an alumina tube using a glass seal (Aremco 617). The anode electrode was exposed to humidified H_2–CH_4 mixed and humidified CH_4 atmospheres with a constant flow rate of 50 mL min^{-1} (a room temperature bubbler was used to humidify the fuels). Also, extra dry air flowed through the cathode electrode at a similar rate. The electrochemical behavior of the cells was studied by ac impedance spectroscopy, potentiodynamic analysis and potentiostatic analysis (Solartron frequency response analyzer 1255 in combination with a Solartron electrochemical interface 1287) at 800, 850 and 900 °C on fuel cells with a four-electrode configuration. Impedance measurements were carried out under open circuit condition over a frequency range from 0.1 Hz to 100 kHz with a 10 mV ac perturbation.

2.3. Cell characterization

The microstructure of the electrodes both before and after electrochemical testing was examined on fractured surfaces with a JEOL 6301F field emission scanning electron microscope (FE-SEM). Bulk phase study was done by XRD and surface analysis was performed by X-ray photoelectron spectroscopy (XPS) (Axis 165 X-ray photoelectron spectrometer, Kratos Analytical).

3. Results and discussion

Conducting extensive symmetrical cell studies, we investigated the electrochemical behavior of WC-based anodes prior to this work [26]. To effectively study carbide-based anode materials, a reasonably active cathode had to be chosen. At first, a platinum cathode was picked. To solely characterize the performance of the Pt cathode, a Pt symmetrical cell was made. Fig. 1 shows the ac impedance spectra of this symmetrical cell at 800 and 900 °C. As clearly observed, the performance of such a cathode is rather poor. We then compared the symmetrical Pt cell with a symmetrical LSM infiltrated porous YSZ support cell, which is also illustrated in Fig. 1. Since the performance of the latter is dramatically better, it was picked as the cathode of choice for the entire study.

Fig. 2 shows the electrochemical performance of a conventional WC-YSZ and a WC-infiltrated porous YSZ anode including (a) open circuit impedance spectra, (b) an equivalent circuit model, and (c) V–i characteristics and power densities at 800 °C under humidified 80% H_2–20% CH_4 mixed atmosphere and humidified methane. As discussed elsewhere [26], the carbide phase is not stable under pure hydrogen fuel and sluggishly decomposes to tungsten metal. To preserve the carbide phase under open circuit condition, a slight amount of methane (>2.5%) must be introduced into the humidified hydrogen atmosphere. That is why humidified 80% H_2–20% CH_4 mixed atmosphere is used as a hydrogen rich fuel.

Using similar methodology, we have extensively studied the electrochemical behavior of symmetrical LSM infiltrated YSZ cathodes [28] and that of symmetrical WC-based anodes [26]. Considering the fact that the polarization resistance of the LSM cathode under OCP is very low (about 0.15 Ω cm^2), the rather large polarization resistance of such a cell can be reasonably attributed to the anode electrode. It is noteworthy that the characteristics of the impedance spectra of the fuel cell strongly resemble that of the symmetrical WC-based one. As observed in Fig. 2, no matter whether the cell is conventional or infiltrated, the impedance comprises two semicircles: a small arc in the high frequency range and a relatively large arc in the low frequency range. This is also the case for both the mixed and methane atmospheres. To attribute the semicircles, an equivalent circuit is shown in this Fig. 2(b) which includes the ohmic resistance corresponding to the YSZ electrolyte (R0), and the non-ohmic polarization corresponding to the composite electrode (R1 and R2). Table 1 summarizes the resistances for the conventional cell and the infiltrated one based on the fit data. The small arc in the high-medium frequency range is predominantly attributed to charge transfer resistance (R1) corresponding to electron transfer and ion transfer processes occurring

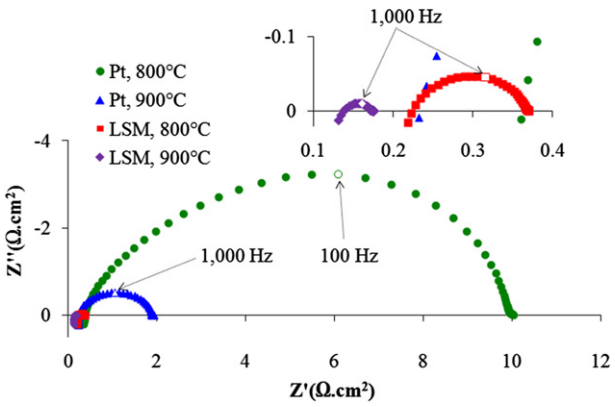

Fig. 1. Comparison between a conventional Pt cathode and a LSM infiltrated porous YSZ cathode.

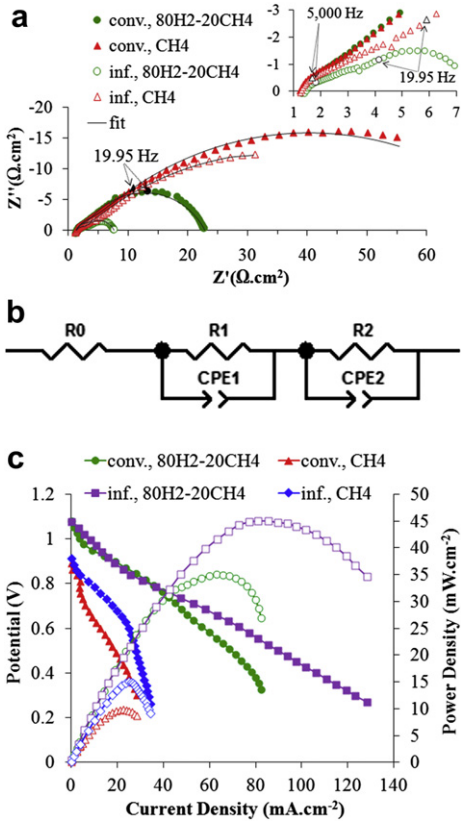

Fig. 2. Performance of cells with a conventional WC-YSZ composite anode and a WC-infiltrated porous YSZ anode at 800 °C (a) Ac impedance spectra, (b) An equivalent circuit, and (c) *V*–*i* characteristics.

at the interfaces [26]. The large arc in the low frequency range of the impedance spectra can be attributed to non-charge transfer processes including surface reactions and solid state and gas phase diffusion [26]. As shown in Table 1, the non-charge transfer resistance (R2) is affected by the type of cell (conventional or infiltrated) to a great extent. Also, it varies remarkably from hydrogen rich fuel to methane fuel. Since a gas diffusion limitation is not expected under OCV conditions, it is suggested that the low frequency arc is due to anodic surface reactions [29]. Consequently, the large difference between R2 under hydrogen rich and methane fuels for both cell types is mainly because methane is much harder to activate at 800 °C [26].

In general, the performance of WC-YSZ anodes is relatively poor, particularly toward methane fuel. For example, the total electrode polarization, which is the difference between the high frequency and low frequency intercepts with the real axis (R1 + R2), under mixed fuel at 800 °C is 21.5 and 6.2 Ω cm^2 for conventional and infiltrated cells, respectively (Fig. 2(a)). *V*–*i* characteristics of these cells also suggest that cells based on WC-YSZ anodes performed weakly. The maximum power densities at 800 °C were 35 and 45 mW cm^{-2} under mixed fuel, and as low as 10 and 15 mW cm^{-2} under methane.

Table 1
Ohmic and non-ohmic polarization resistance of cells based on conventional and infiltrated carbide anodes.

Name	R0 (Ω cm^2)		R1 (Ω cm^2)		R2 (Ω cm^2)	
	80–20 mix	CH_4	80–20 mix	CH_4	80–20 mix	CH_4
Conventional WZ	1.30	1.25	1.35	1.50	20.15	74.85
Infiltrated WZ	1.40	1.25	1.45	1.10	4.75	66.45

The comparison between conventional and infiltrated WC-YSZ, however, was really informative and several observations should be noted here. Firstly, although the amount of the carbide phase was much less in the infiltrated cell (20 vol.% as opposed to 50 vol.% in the conventional cell), the performance was better. Fig. 3 shows the XRD spectra for a conventional WC-YSZ (50 vol.% WC) and an infiltrated one (20 vol.% WC). The remarkable broadening in WC diffraction peaks is due to a great decrease in carbide phase crystal size. The calculated crystal size of WC using XRD line broadening and the Scherrer equation was about 55 and 10 nm for conventional and infiltrated samples, respectively. This suggests that the surface area of the latter should be considerably higher which can contribute to improved performance.

In addition, the stability of conventional and infiltrated cells is quite different. Fig. 4 shows how the power density varies over a period of 18 h under potentiostatic condition (cell voltage = 0.7 V) in both conventional and infiltrated cells at 850 °C in 80% H_2–20% CH_4 mixed fuel. While the conventional cell performed quite stably for the first hour, it experienced a noticeable power decrease over the next 2 h and then stayed relatively constant. The infiltrated cell, however, experienced a great power increase in the first half of the experiment followed by a stable performance in the second half. To cast light on this, the impedance spectra of these cells are illustrated in Fig. 5 before and after the stability test. Comparing the impedance spectra, a remarkable increase in ohmic resistance is observed (from 0.8 to 1.65 Ω cm^2) in the conventional cell (Fig. 5(a)). Also, as for the polarization arcs, a great increase is observed in the first semicircle (high frequency arc), while the second one (low frequency arc) is relatively unchanged. After this test, once the sample was cooled down and removed from the cell, the anode electrode was delaminated and detached from the electrolyte (Fig. 5(c)). Thus, the remarkable increase in ohmic resistance is essentially due to the WC-YSZ electrode delamination. Since the high frequency semicircle is attributed to charge transfer polarization corresponding to electron transfer and ion transfer processes occurring at the interfaces [30,31], such delamination also contribute to the marked increase in the high frequency arc.

On the other hand, the behavior of the infiltrated cell was different. As illustrated in Fig. 5(b), the increase in ohmic resistance after the stability test is much lower. Since no tungsten oxide phase was detected in the carbide electrode after testing (to be shown later) and the infiltrated electrode was well attached to the electrolyte, such an increase in ohmic resistance is most probably due to contact resistance with the gold current collector. As opposed to the conventional cell, while the high frequency arc in the infiltrated sample is relatively unchanged, a rather large increase in the low frequency arc is observed. As discussed elsewhere [26], surface oxidation of the carbide phase is one of the two possible mechanisms of the fuel oxidation process. Before the sample is polarized, the fresh surface layer of the carbide nano-particles is very active

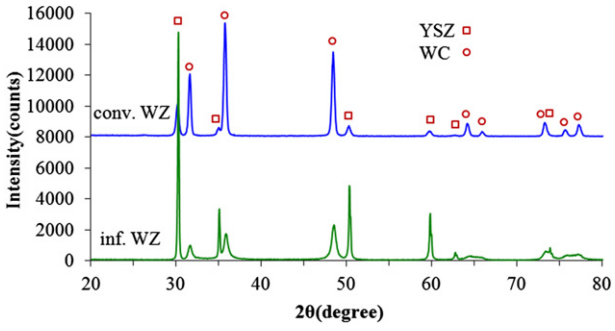

Fig. 3. XRD spectra of the conventional and infiltrated WC-YSZ composite.

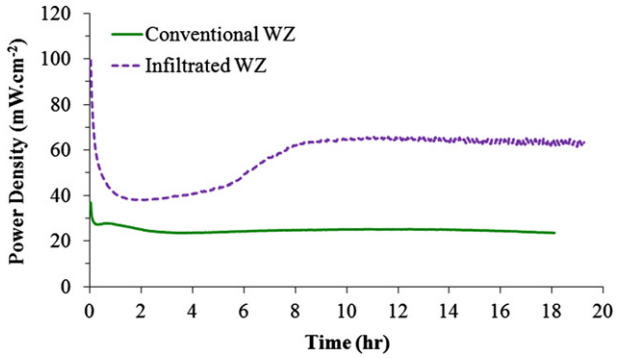

Fig. 4. Potentiostatic performance (0.7 V) of cells with the conventional WC-YSZ composite anode and a WC-infiltrated porous YSZ anode under humidified mixed fuel at 850 °C.

toward the fuel. Once the cell is polarized for 18 h, however, the carbide surface approaches an equilibrium oxidation state. That is why the low frequency arc which is predominantly attributed to non-charge transfer processes including surface reactions [30,32] experiences a rather large increase. This argument is more meaningful when power densities of this cell are considered which were 215 and 84.5 mW cm^{-2} before and after the stability test at 850 °C in mixed fuel, respectively (not shown here).

The XRD spectra of the delaminated conventional carbide electrode and the infiltrated one are shown in Fig. 6. Interestingly, in both the conventional and infiltrated samples, nearly all of the WC phase decomposed to tungsten metal. Cheng et al. [25] explained that the Mo and W metals are more stable in the

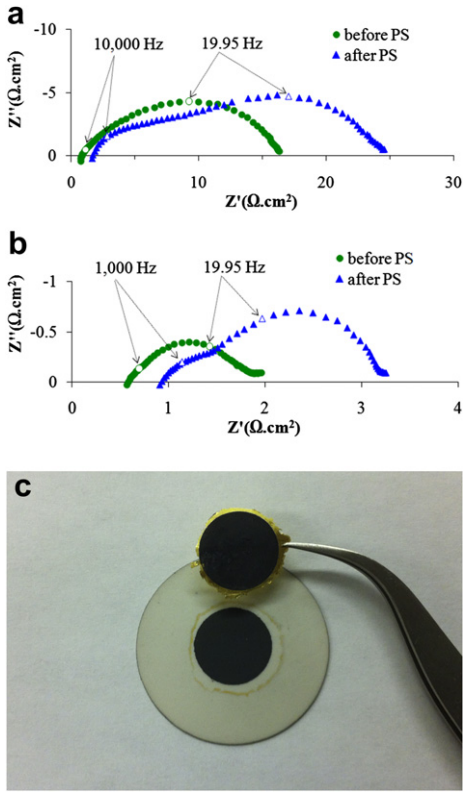

Fig. 5. (a) and (b) Ac impedance of a cell with conventional WC-YSZ composite anode and WC-infiltrated porous YSZ anode before and after a potentiostatic test under humidified mixed fuel at 850 °C, (c) anode delamination in the conventional sample.

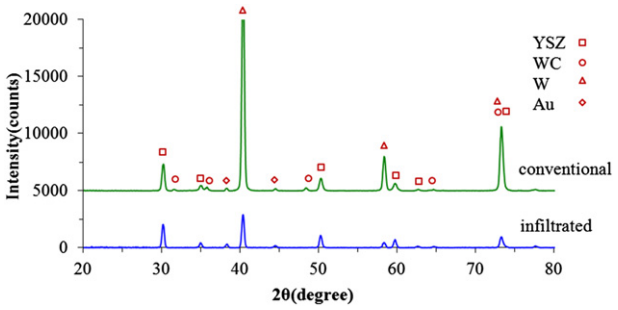

Fig. 6. XRD spectra of the conventional and infiltrated WC-YSZ composite after a potentiostatic test under humidified mixed fuel at 850 °C.

reducing SOFC anode atmosphere. They, however, considered hydrogen-based fuel. We previously discussed [26] that WC was not stable under hydrogen and decomposed to W. Accordingly, we utilized a 80% H_2–20% CH_4 mixed atmosphere not only to stabilize the carbide phase in the conventional cell, but also to synthesize tungsten carbide in the infiltrated cell. Thermodynamically, one possible reaction which leads to the decomposition of WC is:

$$WC + H_2O = W + CO + H_2 \quad (1)$$

The standard Gibbs free energy for this reaction at 850 °C is + 11.4 kJ mol^{-1} and the equilibrium partial pressure of CO is 0.009 atm. On the other hand, since the fuel atmosphere is humidified 80% H_2–20% CH_4, a recarburization reaction may be written as follows:

$$W + CH_4 = WC + 2H_2 \quad (2)$$

Considering the partial pressure of methane and hydrogen, the Gibbs free energy for such reaction at 850 °C would be −60.5 kJ mol^{-1} which is thermodynamically quite favorable. Thus, the fact that WC did decompose to W under polarization condition should be the inevitable corollary of kinetic factors. Note that such decomposition is responsible for the delamination of the carbide-based electrode in the conventional cell. Since the density of tungsten carbide and tungsten are 15.8 and 19.25 g cm^{-3}, respectively, decomposition causes a volume change of more than 20% and results in delamination of the anode electrode from the electrolyte. Fig. 7 shows the anode/electrolyte interface for a partly delaminated WC-YSZ electrode. As can be readily observed, not only is the anode layer detached from the electrolyte due to the internal stress caused by the volume change in the W-based phases, but several micro-cracks can also be detected within the YSZ

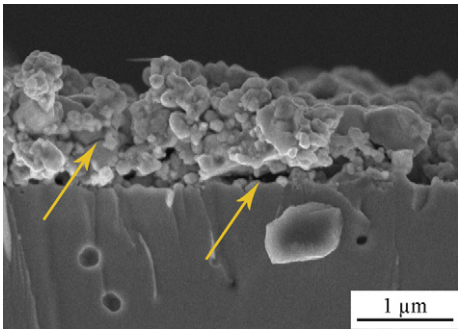

Fig. 7. SEM micrograph of the conventional WC-YSZ anode and YSZ electrolyte interface after a cell test.

particles! Although such decomposition also occurred in the infiltrated sample, the anode stayed well attached to the electrolyte. In the conventional WC-YSZ anode, the carbide phase is actually a structural component of the electrode. However, in the infiltrated cell, only porous YSZ contributes to the structural support and therefore, the volume change of infiltrated carbide particles does not affect the cell's integrity.

When we considered investigating WC-based anode materials, one of the motivations was that we did not expect a carbide-based anode to promote carbon formation under hydrocarbon fuels. In practice, close visual inspection of the studied cells did not reveal any sign of carbon formation or coking under methane. The XPS spectra of carbon (C1s) in as-received WC powder and on a WC-YSZ anode surface is illustrated in Fig. 8. The C1s spectrum of the former was fitted to two peaks including a carbidic type (BE = 283.0 eV, fwhm = 0.7 eV) and a graphitic type (BE = 284.7 eV, fwhm = 1.6 eV). The C1s spectrum of the latter, however, was fitted to three peaks including a carbidic type (BE = 283 eV, fwhm = 1 eV), a graphitic type (BE = 284.4 eV, fwhm = 1.7 eV) and an aromatic type (BE = 285 eV, fwhm = 4 eV). The formation of condensed aromatics has also been reported by others [33,34]. Considering the fact that the WC-YSZ electrode was tested in humidified methane for 12 h at 800 °C under open circuit condition, comparison between these two spectra confirms that coking is not promoted on the carbide phase.

As discussed above, the performance of the WC-YSZ anodes is rather poor particularly toward methane fuel and needs to be improved by incorporation of active electrocatalysts. Furthermore, it has been previously shown [26] that not only can incorporation of electrocatalysts contribute to an improved performance, but it can also affect the stability of the carbide phase. Fig. 9 illustrates the impedance spectra of an infiltrated WC-YSZ cell which was impregnated with 5 wt.% ceria and 1 wt.% Ru (inf-RCWZ) at 800, 850 and 900 °C under humidified 80% H_2–20% CH_4 mixed atmosphere and humidified methane, measured at open circuit voltage. As expected, a great improvement in non-ohmic polarization of the ceria–Ru infiltrated cell is observed particularly under methane. For example, the total electrode polarization (difference between the high frequency and low frequency intercepts with the real axis) under methane at 800 °C is 60.7 and 3.0 Ω cm^2 (the low frequency intercept was measured by a fit semicircle) for the infiltrated WC-YSZ cell, respectively, with and without ceria–Ru. It is noteworthy that the primary change that occurred upon the addition of

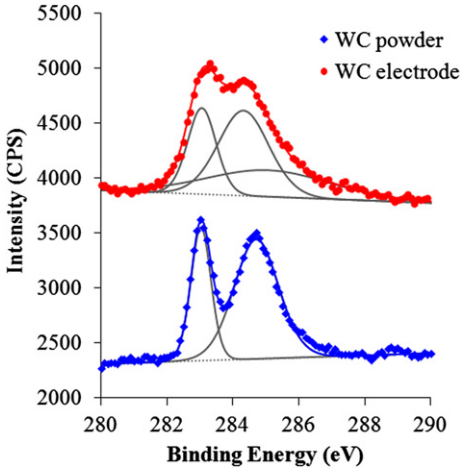

Fig. 8. XPS spectra of elemental carbon (C1s) in as-received WC powder and a WC-YSZ anode surface after cell test under humidified methane at 800 °C.

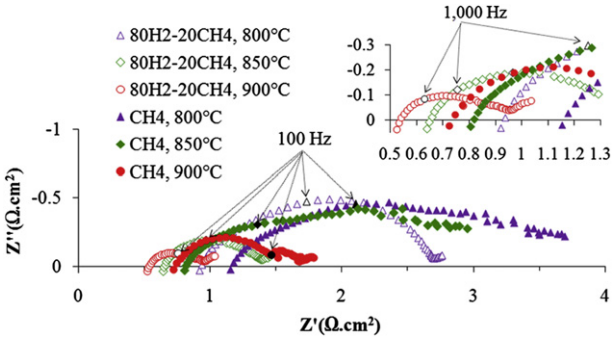

Fig. 9. Ac impedance spectra of a cell with a ceria–Ru promoted WC-infiltrated porous YSZ anode.

ceria–Ru was a dramatic decrease in the semicircle located in the lower frequency range (<100 Hz).

The corresponding *V*–*i* polarization and power density curves of infiltrated RCWZ are shown in Fig. 10 under (a) mixed atmosphere and (b) methane. Note that these polarization measurements were all made after the cells stabilized to be certain of the reproducibility of the results. This is important because, in some cases, the performance was almost twice as high before the cell stabilized. In order for cells to stabilize, they operated under potentiostatic condition (0.7 V) for a period of 24 h at 850 °C in the mixed atmosphere. Furthermore, the ohmic resistance of the relatively thick electrolyte was not compensated in any of the reported results. Interestingly, incorporation of only 5 wt% ceria and 1 wt% Ru into the infiltrated WC-YSZ anode greatly improved the performance. For example at 850 °C, the power density increased from 85 to 185 mW cm^{-2} under hydrogen rich fuel and from 19 to 58 mW cm^{-2} under the methane fuel. As Gross et al. [35] pointed out, compared to higher molecular weight hydrocarbons, methane is rather difficult to activate. Thus, it is clear that the performance of the carbide-based cell under methane fuel is essentially limited by the ability of the anode to break the strong C–H bonds. While the WC-YSZ anode was not effective in methane activation, the Ru-CeO_2-WC-YSZ anode performed with a reasonable activity toward methane fuel.

Fig. 11 compares the measured open circuit voltage of the infiltrated RCWZ under humidified methane and the calculated OCV for hydrogen oxidation from the Nernst equation. As observed, the measured OCV values for methane fuel linearly decrease with increasing temperature. Interestingly, the measured OCV agrees reasonably well with the calculated hydrogen oxidation reaction. McIntosh et al. [36] and Liu and Barnett [37] showed that OCV measurements can provide some insight into the anode reactions. McIntosh et al. [36] argued that since the measured OCVs for a C–Pd–CeO_2-YSZ anode were higher than that of calculated ones over the range of steam-reforming H_2:H_2O ratios, an equilibrium reaction with reformate products was not theoretically possible. In our case, however, not only were the measured OCVs at various temperatures smaller (ΔV ~0.08 V), they also followed a similar trend with increasing temperature. Additionally, our thermodynamic calculation revealed that if only 16% of the H_2O participates in the steam-reforming reaction:

$$CH_4 + 2H_2O = CO_2 + 4H_2 \quad (3)$$

the OCV would decrease from 0.98 to 0.90 V at 800 °C. Although the water content in humidified methane was just 3%, the required H_2O conversion was low enough to possibly occur over the Ru–CeO_2-WC-YSZ anode. It is noteworthy that, in practice, more than one anode reaction may simultaneously

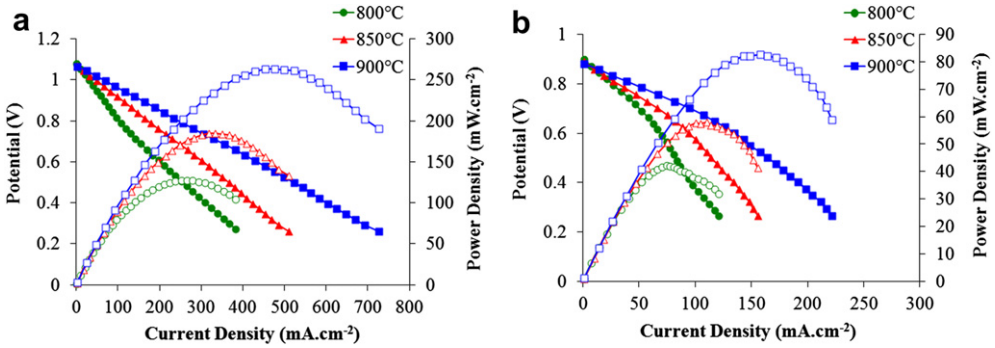

Fig. 10. *V–i* characteristics and power densities of a cell with the ceria–Ru promoted WC-infiltrated porous YSZ anode under (a) Humidified H_2–CH_4 mixed atmosphere and (b) Humidified CH_4.

occur and the experimental OCV may be established by an equilibrium composition.

Fig. 12 shows SEM micrographs (low and high magnification) of the Ru–CeO_2-WC-YSZ anode after a 72 h fuel cell test at different temperatures and under various fuels. WC, ceria and Ru nanoparticles are supported on a porous YSZ backbone. There is a well connected nano-sized WC network intimately seated on the YSZ support. Although Cheng et al. [25] mentioned that a high processing temperature could pose a challenge in Mo- and W-based carbides, it is shown here that the infiltration technique can be effectively used to address the issue. Note that since the carbide phase was formed in-situ, the maximum treatment temperature was only 900 °C. EDS chemical analysis on more than 10 spots confirmed that ceria and Ru were well distributed over the WC-YSZ composite. Overall, the normalized wt% of ceria and Ru were 3.9 and 0.94, respectively. Also, the chemical analysis helped to distinguish among the infiltrated particles. In the high magnification micrograph, WC is the nano-sized well connected network, ceria nano-particles are the smallest (10–20 nm), and Ru particles are rather larger and less populated.

Addition of ceria and Ru electrocatalysts also affects stability of the carbide phase. It was explained earlier that in a conventional WC-YSZ cell, the performance degraded over time during a 24 h potentiostatic test. Based on the post-test analysis, the performance degradation was attributed to gradual delamination of the anode electrode due to the carbide phase decomposition. The performance of a cell with a ceria–Ru impregnated conventional WC-YSZ (con-RCWZ) anode at 850 °C under humidified 80% H_2–20% CH_4 mixed fuel is illustrated in Fig. 13(a). As opposed to the cell with no ceria–Ru, the con-RCWZ cell performed with reasonable stability over a period of 48 h. Fig. 13(b) shows the OCV impedance spectra of the cell before and after the stability test. Interestingly, while the high frequency range arc was almost unchanged, the low frequency range semicircle decreased markedly after the test. Note that a slight increase in the ohmic resistance (from 0.73 to 0.91 Ω cm^2) is most probably due to sluggish sintering of gold particles in the current collector film. As the stability result implied, in contrast with the WZ cell, no delamination occurred in the con-RCWZ cell.

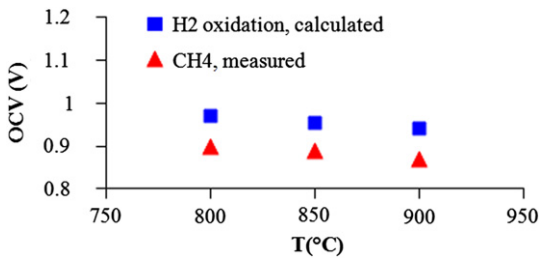

Fig. 11. Comparison between the measured OCV of a cell with the ceria–Ru promoted WC-infiltrated porous YSZ anode under humidified methane and the calculated OCV for hydrogen oxidation from the Nernst equation.

Post phase analysis of the cell revealed that tungsten carbide remained as the major phase besides YSZ. The XRD spectrum of the con-RCWZ cell is shown in Fig. 14. The amount of tungsten metal was quite minor. In addition, a small amount of WO_2 phase was detected. As discussed earlier, our thermodynamic calculation indicated that the carbide phase remains stable under the mixed fuel and we attributed the decomposition of WC to kinetic factors. The fact that the carbide phase remained rather stable in the presence of ceria–Ru electrocatalysts could also support this argument.

Undoubtedly, a key feature of SOFCs in comparison to other fuel cell systems is the ability to internally reform hydrocarbon fuels and to then utilize the produced H_2 and CO, along with the possibility to directly utilize hydrocarbon fuels (direct oxidation). Nevertheless, the build-up of carbon caused by hydrocarbon pyrolysis is a fundamental challenge associated with hydrocarbon fuel utilization particularly with Ni-based anodes as the state-of-the-art anode materials [38,39]. Our primary goal in studying carbide-based materials as alternative anodes for SOFC application was, therefore, to directly utilize hydrocarbons. Knowing the fact that the catalytic attributes of Groups IV–VI carbides are highly similar to those of Pt-group precious metals [20], particularly in reactions which deal with the transformation of C–H bonds of hydrocarbons, we were intrigued to investigate how it would perform under hydrocarbon fuels. This, nonetheless, was not the only motivation to study WC. Although it is a ceramic, the electronic conductivity of tungsten carbide is similar to that of metals (0.52×10^5 S cm^{-1} for WC vs. 1.43×10^5 S cm^{-1} for Ni at room temperature). Moreover, the very high melting point of WC (2870 °C) could virtually guarantee the microstructural stability over long-term operation at high temperatures.

As shown earlier, however, the WC-YSZ anode performed very poorly under methane. Although the carbide-infiltrated anode showed a slight performance improvement, it was still not promising. Addition of highly active electrocatalysts was then essential to enhance the performance. The incorporation of 5 wt% ceria and 1 wt% Ru into the carbide-based anode promoted the performance by a factor of 3. We are aware that these results are still below some reported values in the literature [35,40,41]. However, considering the fact that our cells were electrolyte supported and our results were not compensated, we feel there is certainly room for increasing the power output. For example, the synthesis conditions of the carbide phase should be optimized. Moreover, potentially more effective electrocatalysts (such as doped ceria and/or Pd) need to be investigated. Also, since methane is known to be difficult to activate, other fuels in which the C–H bond can be broken more easily should also be studied.

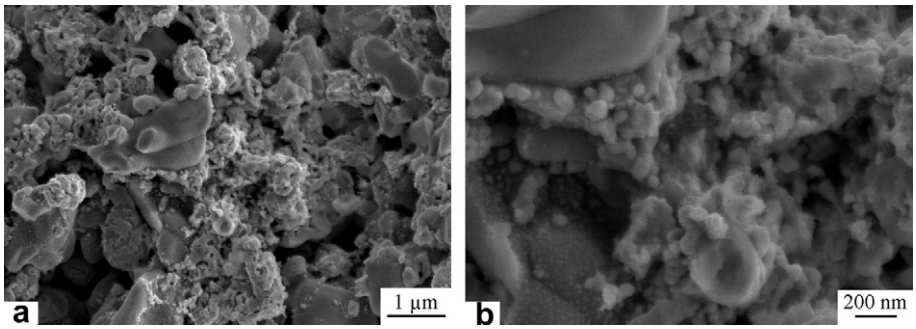

Fig. 12. SEM micrographs of the ceria–Ru promoted WC-infiltrated porous YSZ anode.

In addition to poor performance, instability of the carbide phase posed another challenge which perhaps was even more important. Trying to thoroughly understand the stability issue, we previously [26] performed several ex-situ tests in which WC was exposed to various reforming gases, including H_2 and CO as reducing and carburizing gases and H_2O and CO_2 as oxidizing gases. The ex-situ results showed that WC remained the major phase. Only a very minor amount of WO_x (3–4 wt% when $(H_2O + CO_2)/(H_2 + CO)$ was as high as 2.63) was detected and no decomposition from carbide to metal occurred. In the present work, we tested more than 20 different cells including conventional WC-YSZ, infiltrated WC-YSZ, conventional WC-YSZ with ceria–Ru and infiltrated WC-YSZ with ceria–Ru. Depending on the fuel atmosphere, polarization condition and temperature, the W-based components were quite varied. Earlier, we presented some of the post-analysis XRD results (Figs. 6 and 14). Table 2 presents a conclusive summary of the phase analysis results.

Several important points should be noted from the data in Table 2. First, in the WZ-YSZ anode, a major phase change occurred from carbide to metal. Such a major phase change imposes serious mechanical stress on the anode/electrolyte interface due to a 20% volume change within the anode microstructure and, therefore, results in anode/electrolyte delamination. Second, although such a major phase change similarly occurred in the infiltrated WC-YSZ anode, it did not bring about any delamination. Note that in infiltrated WC-YSZ, the carbide is supported over a consolidated YSZ backbone and essentially does not have any structural attributes. Thus, the volume change is not problematic anymore and no delamination is observed. Third, addition of ceria–Ru electrocatalyst effectively preserved WC as the major phase and both metal and oxide phases remained minor. Finally, no oxide phase was detected in samples tested under hydrogen–methane mixed fuel, while a minor oxide phase was nearly always present in samples tested under methane.

Recently, many attempts have been made to utilize WC and Mo_2C for steam and dry reforming of methane [42–45]. Claridge et al. [42] showed that at atmospheric pressure, the carbide catalyst deactivated due to oxidation reactions and indicated that such deactivation was predominantly governed by kinetics. They also indicated that methane conversion over a carbide catalyst can be explained by two different pathways: a redox mechanism and a noble metal mechanism, which both must participate in the overall reforming reaction. Here, with a similar approach, we list possible reactions for electrochemical oxidation of hydrogen and methane over WC. Once the cell is polarized, the following reactions could possibly happen on the carbide surface:

$$O^{-2} = O^* + 2e^- \quad (4)$$

$$H_2 = 2H^* \quad (5)$$

$$CH_4 = C^* + 2H_2 \quad (6)$$

$$O^* + 2H^* = H_2O \quad (7)$$

$$O^* + C^* = CO \quad (8)$$

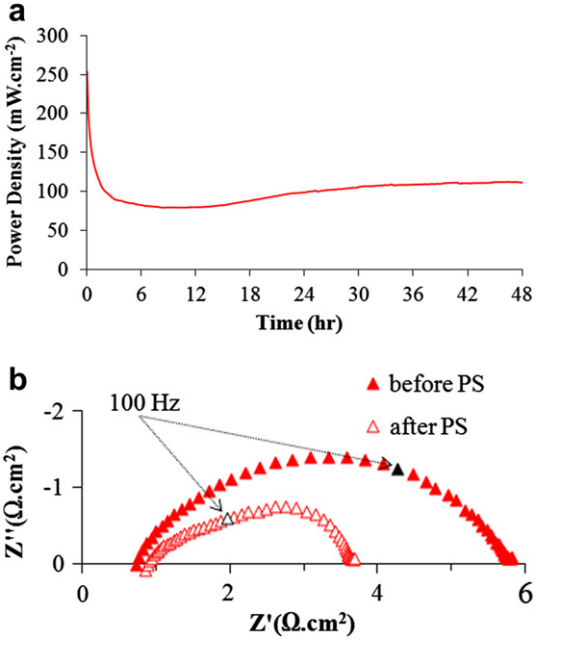

Fig. 13. (a) Potentiostatic performance (0.7 V) of a cell with the ceria–Ru impregnated conventional WC-YSZ anode at 850 °C under mixed fuel, (b) OCV impedance spectra of the cell before and after the stability test.

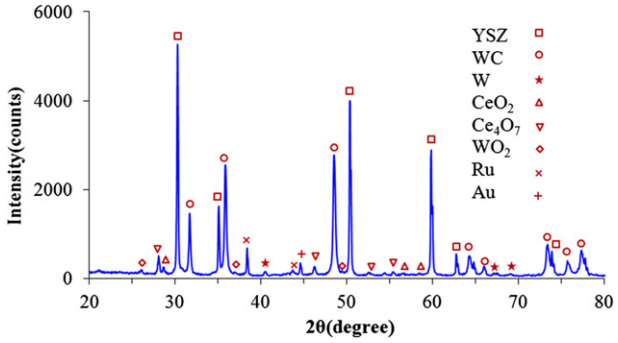

Fig. 14. XRD spectra of a cell with the ceria–Ru impregnated conventional WC-YSZ anode after a potentiostatic test under humidified mixed fuel at 850 °C.

Table 2
Summary of the phase analysis after fuel cell test (M: major phase, m: minor phase).

W-based component	WC-YSZ		Ru–CeO_2-WC-YSZ	
	H_2–CH_4	CH_4	H_2–CH_4	CH_4
WC	m	m	M	M
W	M	M	m	m
WO_x	–	m	–	m

$$WC + O^* = W\_ + CO \quad (9)$$

$$W\_ + C^* = WC \quad (10)$$

$$W\_ + O^* = WO \quad (11)$$

$$WO + 2H^* = W\_ + H_2O \quad (12)$$

In the redox mechanism, once the charge transfer reaction of the oxygen ion takes place, the corresponding oxygen atom (O^*) adsorbs on the carbide surface and reacts with the carbon in the carbide surface (Eq. (9)). A carbon vacancy (W_) is created as a result of this reaction. The vacancy is then filled with either carbon or oxygen (Eqs. (10) and (11)). The adsorbed oxygens (O^*) may also react with the active carbon species (C^* from Eq. (6), which is known as the noble metal mechanism Eq. (8)). Note that in the latter mechanism, the surface carbon atoms from the carbide phase are not involved in the mechanism and the carbide phase remains stable.

In the conventional WC-YSZ anode, since a major amount of the carbide phase was decomposed to tungsten metal (Fig. 6), it can be reasonably concluded that the rate of reactions 9 and 12 is greater than that of reactions 10 and 11. In the ceria–Ru infiltrated WC-YSZ electrode, however, the carbide remained as the major phase and the detected metal and oxide phases were very minor. Accordingly, one can conclude that the addition of ceria–Ru could highly enhance the recarburization reaction via Eq. (10), and/or promote the noble metal mechanism to protect carbon atoms in WC (Eq. (8)).

Since, to the best of our knowledge, the current work is one of the initial investigations on potential application of carbide-based materials for SOFC anodes, a reasonable question to be addressed is how promising WC could be as an SOFC anode alternative. Obviously, the major advantages of WC include very high electronic conductivity, great stability at high operating temperature and resistance to carbon formation. In addition, compatibility with precious metals such as Pd and Ru, which are excellent catalysts for hydrocarbon oxidation, can be very beneficial (as is not the case for Cu-based anodes, for example). However, as reported here, although catalytic resemblance between WC and precious metals is well acknowledged [20] and clearly can be quite advantageous, the WC-based anode did not show reasonable performance toward methane fuel on its own and needed to be promoted by other electrocatalysts. Furthermore, since any major phase change from the carbide to either the metal or oxide could irreversibly degrade the performance, stability of WC can pose a serious challenge.

Based on this study, we think the carbide-infiltrated YSZ support can be reasonably considered as a foundation for future studies. First, with a very simple and practical infiltration technique, more than 20 vol.% of the carbide can be incorporated into the porous support. Second, it eliminates the need for a high processing temperature. Third, since the final carbide network is essentially nano-sized, the performance can be promoted. Finally, if any phase change occurs in the carbide phase, the integrity of the YSZ backbone remains intact and a potential permanent degradation can be avoided.

4. Conclusions

The following conclusions could be drawn from the current study:

1. Conventional WC-YSZ composites cannot be considered as a potential alternative anode for direct methane utilization. Not only do they show rather poor performance under methane, but they also experience a major phase change resulting in anode/electrolyte delamination.
2. Cells with a WC-infiltrated YSZ support show a slightly better performance relative to those with conventional WC-YSZ. They also perform stably and tolerate the internal stress caused by any phase change in WC.
3. Incorporation of 5 wt% ceria and 1 wt% Ru significantly improves the performance. Also, the presence of ceria–Ru can effectively preserve WC so that it does not go through a major phase change.
4. The WC-infiltrated YSZ support can be considered as a foundation for further investigation into carbide-based anode materials.

Acknowledgments

This work was financially supported by the Natural Sciences and Engineering Research Council of Canada (NSERC). The authors would also like to acknowledge Dr. Kasra Nikooyeh for his comments on OCV data analysis.

References

[1] A. Atkinson, S. Barnett, R.J. Gorte, J.T.S. Irvine, A.J. McEvoy, M. Mogensen, S.C. Singhal, J.M. Vohs, Nat. Mater. 3 (2004) 17.
[2] Z. Cheng, J.H. Wang, Y.M. Choi, L. Yang, M.C. Lin, M. Liu, Energy Environ. Sci. 4 (2011) 4380.
[3] A.J. Jacobson, Chem. Mater. 22 (2010) 660.
[4] C. Sun, U. Stimming, J. Power Sources 171 (2007) 247.
[5] J.B. Goodenough, Y.H. Huang, J. Power Sources 173 (2007) 1.
[6] W.Z. Zhu, S.C. Deevi, Mater. Sci. Eng. A 362 (2003) 228.
[7] M.D. Gross, J.M. Vohs, R.J. Gorte, J. Mater. Chem. 17 (2007) 3071.
[8] M.L. Toebes, J.H. Bitter, A.J. van Dillen, K.P. de Jong, Catal. Today 76 (2002) 33.
[9] M. Cimenti, J.M. Hill, Energies 2 (2009) 377.
[10] K. Haga, S. Adachi, Y. Shiratori, K. Itoh, K. Sasaki, Solid State Ionics 179 (2008) 1427.
[11] S.P. Jiang, S.H. Chan, J. Mater. Sci. 39 (2004) 4405.
[12] D. Sarantaridis, A. Atkinson, Fuel Cells 7 (2007) 246.
[13] S. McIntosh, R.J. Gorte, Chem. Rev. 104 (2004) 4845.
[14] H. Kim, S. Park, J.M. Vohs, R.J. Gorte, J. Electrochem. Soc. 148 (2001) A693.
[15] R.J. Gorte, J.M. Vohs, J. Catal. 216 (2003) 477.
[16] J.W. Fergus, Solid State Ionics 177 (2006) 1529.
[17] S.W. Tao, J.T.S. Irvine, Chem. Rec. 4 (2004) 83.
[18] N.Q. Minh, J. Am, Ceram. Soc. 76 (1993) 563.
[19] R.B. Levy, M. Boudart, Science 181 (1973) 547.
[20] H.H. Hwu, J.G. Chen, Chem. Rev. 105 (2005) 185.
[21] Y. Hara, N. Minami, H. Itagaki, Appl. Catal. A 323 (2007) 86.
[22] D.J. Ham, Y.K. Kim, S.H. Han, J.S. Lee, Catal. Today 132 (2008) 117.
[23] R. Ganesan, D.J. Ham, J.S. Lee, Electrochem. Commun. 9 (2007) 2576.
[24] A. Naoumidis, F. Tietz, G. Stochniol, A. Gupta, T. Hauber, Proceedings of the 2nd European Solid Oxide Fuel Cell Forum, Oberrohrdorf, Switzerland (1996) 727.
[25] Z. Cheng, S. Zha, M. Liu, J. Electrochem. Soc. 153 (2006) A1302.
[26] A. Torabi, T.H. Etsell, N. Semagina, Partha Sarkar, Electrochim. Acta 67 (2012) 172.
[27] M.P. Pechini, U.S. Patent No. 3,330,697 (1967).
[28] A. Torabi, A.R. Hanifi, T.H. Etsell, P. Sarkar, J. Electrochem. Soc. 159 (2011) B1.
[29] S. McIntosh, J.M. Vohs, R.J. Gorte, J. Electrochem. Soc. 150 (2003) A1305.
[30] S.B. Adler, Solid State Ionics 111 (1998) 125.
[31] T.L. Reitz, H. Xiao, J. Power Sources 161 (2006) 437.
[32] Q.A. Huang, R. Hui, B. Wang, J. Zhang, Electrochim. Acta 52 (2007) 8144.
[33] F. Larachi, H.O. Hassani, M.C. Iliuta, B.P.A. Grandjean, P.H. McBreen, Catal. Lett. 84 (2002) 183.
[34] H.O. Hassani, S. Rakass, N. Abatzoglou, P. Rowntree, J. Power Sources 171 (2007) 850.
[35] M.D. Gross, J.M. Vohs, R.J. Gorte, J. Electrochem. Soc. 154 (2007) B694.
[36] S. McIntosh, J.M. Vohs, R.J. Gorte, Electrochem. Solid-State Lett. 6 (2003) A240.
[37] J. Liu, S.A. Barnett, Solid State Ionics 158 (2003) 11.

[38] C.M. Finnerty, N.J. Coe, R.H. Cunningham, R.M. Ormerod, Catal. Today 46 (1998) 137.
[39] R. Kikuchi, N. Koashi, T. Matsui, K. Eguchi, T. Norby, J. Alloys Compd 408–412 (2006) 622.
[40] Y. Lin, Z. Zhan, J. Liu, S.A. Barnett, Solid State Ionics 176 (2005) 1827.
[41] Y. Nabae, I. Yamanaka, M. Hatano, K. Otsuka, J. Electrochem. Soc. 153 (2006) A140.
[42] J.B. Claridge, A.P.E. York, A.J. Brungs, C. Marquez-Alvarez, J. Sloan, S.C. Tsang, M.L.H. Green, J. Catal. 180 (1998) 85.
[43] A.R.S. Darujati, D.C. LaMont, W.J. Thomson, Appl. Catal. A 253 (2003) 397.
[44] D.C. LaMont, A.J. Gilligan, A.R.S. Darujati, A.S. Chellappa, W.J. Thomson, Appl. Catal. A 255 (2003) 239.
[45] J. Sehested, C.J.H. Jacobsen, S. Rokni, J.R. Rostrup-Nielsen, J. Catal. 201 (2001) 206.